ACS APPLIED MATERIALS & INTERFACES

Research Article

www.acsami.org

Structural and Permeation Kinetic Correlations in PdCuAg Membranes

Lingfang Zhao, Andreas Goldbach,* Chun Bao, and Hengyong Xu

Dalian National Laboratory for Clean Energy, Dalian Institute of Chemical Physics, Chinese Academy of Sciences, Zhongshan Road 457, 116023 Dalian, China

Supporting Information

ABSTRACT: Addition of Ag is a promising way to enhance the H_2 permeability of sulfur-tolerant PdCu membranes for cleanup of coal-derived hydrogen. We investigated a series of PdCuAg membranes with at least 70 atom % Pd to elucidate the interdependence between alloy structure and H_2 permeability. Membranes were prepared via sequential electroless plating of Pd, Ag, and Cu onto ceramic microfiltration membranes and subsequent alloying at elevated temperatures. Alloy formation was complicated by a wide miscibility gap in the PdCuAg phase diagram at the practically feasible operation temperatures. X-ray diffraction showed that the lattice constants of the fully alloyed ternary alloys obey Vegard's law closely. In general, H_2 permeation rates increased with increasing Ag and decreasing Cu content of the membranes in the investigated temperature range. Detailed examination of the permeation kinetics revealed compensation between activation energy and pre-exponential factor of the corresponding H_2 permeation laws. The origin of this effect is discussed. Further analysis showed that the activation energy for H_2 permeation decreases overall with increasing lattice constant of the ternary alloy. The combination of these correlations results in a structure–function relationship that will facilitate rational design of PdCuAg membranes.

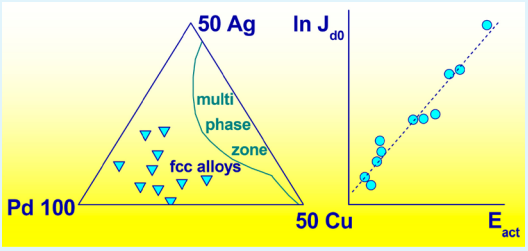

KEYWORDS: *hydrogen separation, ternary alloy, Vegard's law, kinetic compensation, structure–function relationship*

1. INTRODUCTION

Dense Pd-based membranes are widely investigated for H_2 purification and application in membrane reactors.[1−3] In particular, integration into steam reforming and water–gas shift reactors has been frequently studied for small-scale H_2 production.[2−5] Hydrogen is mostly produced from natural gas nowadays, but coal and biomass are much more abundant and evenly distributed worldwide. Hence, the latter are attractive feed stocks for production of H_2 as a clean and sustainable energy carrier.[5] However, syngas derived from coal and biomass usually contains sulfur, which can easily damage many Pd-type membranes. For example, H_2S reacts with Pd and PdAg to form $Pd_{2.8}S$, Pd_4S, and $Ag_5Pd_{10}S_5$, which largely inhibit hydrogen permeation and also cause mechanical membrane failure.[6−8]

Palladium alloys with copper and gold and face-centered cubic (fcc) structure are exceptions in this respect since such membranes exhibit good H_2S tolerance as McKinley discovered nearly 50 years ago.[9] Cu alloys have attracted more attention[6,8,10−13] because Cu also reduces the noble metal costs and enhances low-temperature membrane stability.[14,15] However, hydrogen permeability declines rapidly with increasing Cu content except for a narrow range of highly permeable PdCu alloys with body-centered cubic (bcc) structure, but those do not withstand sulfur well either.[11] There has been a thrust in recent years to improve the permeability of PdCu alloys through addition of Ag[16−21] since PdAg alloys are well known for their excellent H_2 permeability and Ag is a relatively inexpensive noble metal. Density functional theory (DFT) calculations[16] provided trends for hydrogen solubility, diffusivity, and permeability in fcc PdCuAg alloys with Pd ≥ 66% (all compositions are given in atom % in the present study). Yet, experimental validation of those findings is largely missing as laboratory studies on such membranes were limited to a few select compositions with mostly high Cu (20−30%) and moderate to low Ag contents (1−15%).[17−20] Moreover, those reports largely lack characteristic permeation kinetic parameters which are important for both fundamental understanding and practical implementation of such membranes.

The scope of the present work is gaining systematic insight into the structural and permeation kinetic properties of PdCuAg alloys. In addition, we want to understand how membrane characteristics are influenced by alloy formation from sequentially deposited metal layers at moderate annealing temperatures because composite palladium membranes prepared by electroless plating (ELP) on alumina substrates are found to be most promising for practical applications.[1] Accordingly, we prepared a series of PdCuAg/ceramic composite membranes with at least 70% Pd and otherwise Ag-rich, Cu-rich, and approximately even Ag and Cu stoichiometry. Structural analyses and permeation measure-

Received: September 18, 2014
Accepted: December 2, 2014
Published: December 15, 2014

   dx.doi.org/10.1021/am506439x | ACS Appl. Mater. Interfaces 2014, 6, 22408−22416

ments have been carried out during and after completion of alloy formation in the hydrogen-selective metal layer.

2. EXPERIMENTAL SECTION

2.1. Membrane Preparation. Alloy membranes were supported on the outside of commercial ceramic microfiltration membranes (TAMI) provided by the Energy research Centre of the Netherlands (ECN). The outer surface of these tubes with a 14 mm outer (o.d.) and 10 mm inner diameter (i.d.) had been furnished with a macroporous coating at ECN to reduce the average pore size to 3.4 μm.[22] Those pores were blocked with an inorganic filler before metal deposition via electroless plating (ELP) to prevent ingress of Pd into the substrate pores as previously described.[23] Palladium, silver, and copper were plated in this sequence and eventually alloyed at 773−823 K. Substrates were activated with Pd seeds before Pd and Ag deposition and afterward dried for 4 h at 423 K in air followed by 2 h annealing at 723 K in flowing N_2. Copper was plated directly onto the annealed PdAg surface and then dried and annealed as before. Commercial solutions were used for Pd seeding (OPC-50 inducer and OPC-150 cryster, Okuno Chemical Industries) and Pd plating (PALLA TOP, Okuno) and applied as elsewhere detailed.[24] Compositions and operation parameters of the homemade Ag and Cu baths have been described before too.[25,26] The membranes were once turned upside down during each metal deposition step to avoid uneven metal deposition along the up to 15 cm long substrates. Altogether six membranes M1−M6 have been prepared in this way. Using the same procedures, a Pd/Ag/Cu trilayer M7 was prepared on a ceramic membrane tube (8 mm i.d., 12 mm o.d.) supplied by the Nanjing University of Technology for structural alloy formation studies.

Preparation of very thin Pd alloy membranes with precise stoichiometry via ELP is notoriously difficult. Therefore, we determined binary alloy compositions after Pd and Ag deposition and then adjusted Cu plating times to reach ternary target compositions. Practically, we started with 15 cm long support pieces and cut off 1 cm long pieces from each end before and after Cu deposition. These cutoff pieces were labeled top and bottom according to sample end and annealed for 60 h at 1073 K in N_2 for rapid alloying of the metals and subsequent alloy composition analysis. Following PdAg precursor analyses we plated additional Ag or Pd on several membranes in order to get closer to target compositions. In these cases another set of end pieces was cut off for rapid alloying and chemical analysis. After Cu plating the remainder of the membrane tubes was annealed at 773 K in H_2 for 48 h and then transferred to ECN where one end was joined to a stainless steel extension tube and the other one closed off with a stainless steel cap using graphite seals.

2.2. Permeation Measurements. The setup for permeation and alloying experiments has been elsewhere described.[27] Membranes were mounted with graphite gaskets into a stainless steel separator shell which was placed inside a furnace. H_2 (purity > 99%)[28] or N_2 (99.999%) was supplied to the membrane outside, while the tube interior was kept at atmospheric pressure. Sweep gas was not used. Feed gas flow and pressure were set with a mass flow controller in the feed and a back pressure valve in the retentate line, respectively. The feed side pressure P_{feed} was measured with a pressure gauge at the retentate exit. Permeate fluxes were measured with a soap bubble flow meter or an TH-ZM8 electronic soap film flowmeter (Wuhan Tianhong Instrument Co. Ltd.) when permeate volume rates were larger than 1500 mL min^{-1}. Membranes were heated under N_2 at 1 K min^{-1} to 773 K and then annealed at that temperature under flowing H_2 (ca. 150 mL min^{-1}, $P_{feed} \approx 120$ kPa) to form the alloy. From time to time H_2 permeation rates J_{H2} were determined in the range 473−823 K at pressure difference ΔP_{H2} = 100 kPa to determine activation energies. Temperature was changed at a rate of ca. 1.5 K min^{-1} and held at least 40 min constant before fluxes were recorded. The pressure dependence was investigated varying P_{feed} between 150 and 600 kPa.

2.3. Membrane Characterization. Alloyed PdAg precursor and PdAgCu layers from cutoff samples were detached from the ceramic support for structural and compositional analyses. The thickness of the PdCuAg layers was calculated from the area and weight of such fragments. X-ray diffraction (XRD) patterns were recorded with an X'Pert PRO diffractometer (PANalytical) using Cu Kα radiation at 40 kV and 40 mA. Energy-dispersive X-ray spectroscopic analysis (EDS) was carried out on a FEI Quanta 200 F scanning electron microscope equipped with an Ametek detector.

3. RESULTS AND DISCUSSION

3.1. Vegard's Law. Figure 1 displays diffraction patterns of alloyed metal layers from the top cutoff pieces of each ternary membrane. All XRD patterns indicate single-phase fcc structures, and the same was found for the bottom end PdCuAg membrane pieces and all PdAg precursor samples. Table 1 lists experimental lattice parameters for each ternary and binary precursor sample. This allows us to examine whether these ternary metal layers obey Vegard's law.[29] According to this rule the lattice constant a_{alloy} of an alloy is a linear function of the atomic fractions x_{metal} and metal lattice constants a_{metal}. For PdAg and PdCuAg alloys this correlation can be written as follows

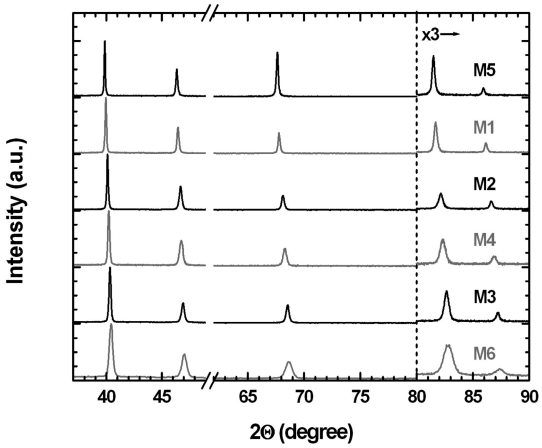

Figure 1. Diffraction patterns of PdCuAg alloys after 60 h annealing under N_2 at 1073 K. The region above 2Θ = 80° is 3-fold magnified.

$$a_{PdAg} = x_{b,Pd}a_{Pd} + x_{b,Ag}a_{Ag} = a_{Pd} + x_{b,Ag}(a_{Ag} - a_{Pd}) \quad (1)$$

$$a_{PdCuAg} = x_{t,Pd}a_{Pd} + x_{t,Ag}a_{Ag} + x_{t,Cu}a_{Cu} = a_{Pd} + x_{t,Ag}(a_{Ag} - a_{Pd}) - x_{t,Cu}(a_{Pd} - a_{Cu}) \quad (2)$$

Since nominal binary atomic fractions, e.g., $x_{b,Ag}$ and $x_{b,Pd}$, in a ternary alloy can be expressed as a function of the ternary ones, i.e., $x_{t,Ag}$ and $x_{t,Pd}$, eqs 1 and 2 can be combined to give

$$a_{PdCuAg} = a_{PdAg} - x_{t,Cu}(a_{PdAg} - a_{Cu}) \quad (3)$$

Figure 2 shows a plot of calculated vs experimental lattice constants for the ternary membrane alloys. Experimental values were determined by averaging the lattice constants derived from the 111, 200, 220, 311, and 222 alloy diffraction peaks of the top cutoff pieces. Theoretical values were calculated on the basis of EDS analyses of the same cutoff pieces (Table 1) employing eqs 1 and 3. Parameters of eq 1 were taken from a previous study (a_{Pd} = 3.887 Å, $(a_{Ag} - a_{Pd}) = 1.93 \times 10^{-3}$ Å, x_{Ag} in %),[24] and a_{Cu} = 3.619 Å was determined from the diffraction pattern of an electroless-plated Cu layer on an ECN support tube after it had been also annealed for 60 h at 1073 K in N_2.

Table 1. Composition Analyses of PdCuAg Membrane Alloys

membrane			PdAg[a]			PdCuAg			
	location	analysis method	a_{PdAg}, Å	Pd, %	Ag, %	a_{PdCuAg}, Å	Pd, %	Ag, %	Cu, %
M1	top	EDS		78.0	22.0		71.9	20.3	7.8
	top	XRD	3.929	78.1	21.9	3.905	71.6	20.0	8.4
	bottom		3.931	77.0	23.0	3.905	69.8	20.8	9.4
M2	top	EDS		86.8	13.2		77.5	11.8	10.7
	top	XRD	3.919	83.7	16.3	3.888	74.3	14.5	11.1
	bottom		3.916	85.2	14.8	3.888	76.5	13.3	10.2
M3	top	EDS		94.9	5.1		81.9	4.4	13.7
	top	XRD	3.898	94.1	5.9	3.869	83.1	5.2	11.8
	bottom		3.898	94.4	5.6	3.871	84.4	5.0	10.6
M4	top	EDS		91.3	8.7		75.9	7.2	16.9
	top	XRD	3.908	88.9	11.1	3.878	78.7	9.8	11.5
M5	top	EDS		80.1	19.9		75.4	18.7	5.9
	top	XRD	3.926	79.6	20.4	3.914	76.1	19.5	4.5
	bottom		3.927	79.4	20.6	3.910	74.6	19.4	6.0
M6	top	EDS		95.3	4.7		78.5	3.9	17.6
	top	XRD	3.897	95.0	5.0	3.856	79.7	4.2	16.1
	bottom		3.897	94.7	5.3	3.860	80.5	4.5	15.0
M7	bottom	EDS		88.8	11.2		80.2	10.1	9.7
	top	XRD	3.918	84.0	16.0				
	bottom					3.888	75.5	14.4	10.1

[a]PdAg binary EDS compositions derived from EDS analyses of ternary samples.

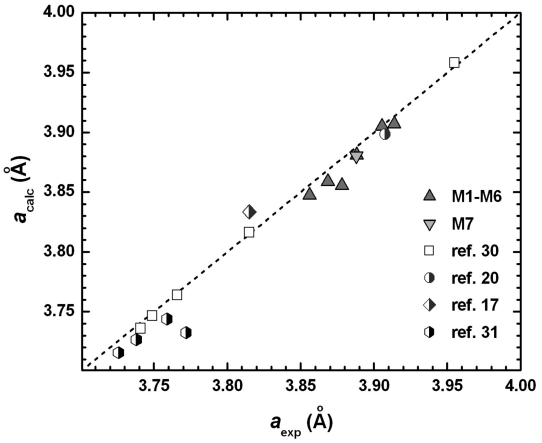

Figure 2. Comparison between experimental lattice constants of PdCuAg alloys and those calculated according to Vegard's law from chemical analyses. The lattice constant of the membrane described in ref 20 was extracted from Figure 2 of that publication.

For comparison, Figure 2 includes experimental lattice constants from fcc PdCuAg alloys reported by Raub and Wörwag, who prepared their samples using high-temperature metallurgical methods.[30] Those values practically fall on the line that marks Vegard's law, suggesting that the latter applies rather well for PdCuAg alloys. The measured lattice constants of the here prepared samples agree within 0.3% with predictions of eq 3 except for M4 which deviates by almost 0.6%. Lattice constants reported for PdCuAg membranes fabricated by sputtering[20] and ELP[17] and PdCuAg thin films prepared by electrodeposition[31] agree similarly well with Vegard's law (Figure 2). Deviations of that magnitude from Vegard's law have been also observed for electrodeposited PdCuAu thin films[32] and PdCu thin films prepared by laser deposition.[33] Guay and co-workers attributed the differences in the as-prepared alloys to lattice strain caused by growth-related structural deformations[31,33] and lattice deformations imposed by the differing atom sizes.[32] The metal atom radii[34] of Ag (1.445 Å) and Au (1.442 Å) are practically identical, so that Ag and Au incorporation should lead to comparable deformations of PdCu crystal lattices. However, the excellent agreement of the metallurgically prepared alloys[30] with Vegard's law implies that PdCuAg alloy lattices can be fully relaxed at high temperatures. Thus, the here employed annealing treatment at 1073 K may not have been sufficient for healing growth-related lattice defects and deformations completely.

Inhomogeneity may have contributed to the deviations from Vegard's law in the present case too, although the consistently larger experimental a_{PdCuAg} values (Figure 2) suggest that the aforementioned systematic effects played a more significant role. Table 1 summarizes results of XRD analyses of the alloyed PdAg precursor and PdCuAg membrane cutoff pieces. It can be seen that overall agreement was excellent between top and bottom XRD compositions. The PdAg precursor alloys agreed within 0.2−1.5 atom %, while the maximum variance increased only to 1.1−2.2 atom % after addition of Cu. Note also the similarly good agreement between binary PdAg compositions that were derived from EDS analyses of ternary alloys from top cutoff pieces and XRD analyses of PdAg precursors from the same membrane end (Table 1). This insinuates that the alloys were rather homogeneous along the whole membrane length, showing that such thin-layered multicomponent membranes can be prepared with reasonable stoichiometric accuracy via ELP. In the following we will refer to the average of top and bottom end XRD analyses when discussing the variation of permeation characteristics with composition.

3.2. Low-Temperature Alloying. Ideally the precursors with separate Pd, Ag, and Cu layers have to be alloyed at less than 823 K because composite membranes tend to develop defects at higher temperatures due to the increasing difference in the thermal expansion of ceramic substrate and ultrathin metal layers. Figure 3 shows the evolution of H_2 flux J_{H2}, N_2 leak rate J_{N2}, and activation energy for H_2 permeation, E_{act},

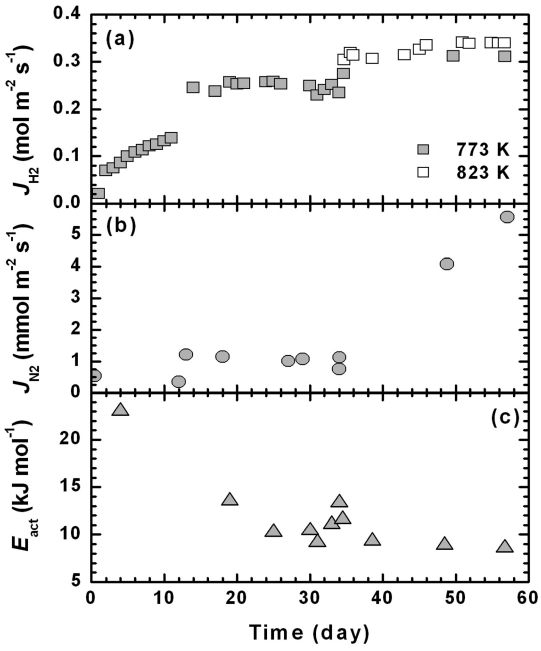

Figure 3. Evolution of (a) H_2 flux, (b) N_2 leak rate, and (c) activation energy for H_2 permeation during alloying of PdCuAg membrane M1 at 773 and 823 K.

during alloying of membrane M1 at 773−823 K. The H_2 flux increased several times abruptly after growing steadily or appearing to be stable for more than a week. This behavior was typical for the here investigated membranes and eventually prompted us to raise the temperature from 773 to 823 K in order to expedite alloy formation. In fact, this process was unexpectedly time consuming since J_{H2} stabilized much faster in our experience during alloying of binary PdAg[25] and PdCu[26] membranes of similar thickness at those temperatures. In general, E_{act} dropped as alloy formation progressed except for temporary increases in connection with the sudden jumps of J_{H2}. The N_2 leak rate remained steady during annealing at 773 K but started to grow after raising the temperature to 823 K.

The structural progress of alloy formation was investigated at 773 K in H_2 using pieces of Pd/Ag/Cu trilayer M7. Figure 4 shows XRD patterns of the ca. 2−3 μm thick layer in differing alloying states. Again, all XRD patterns indicated only fcc

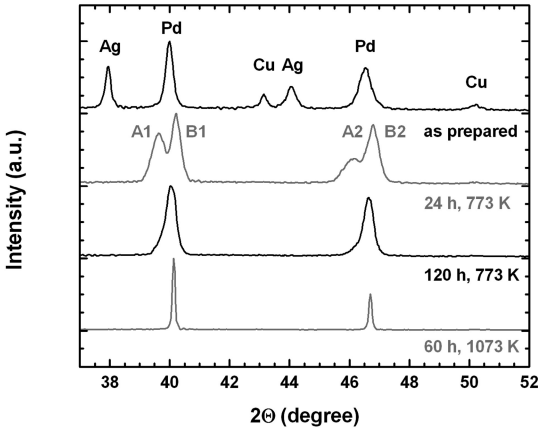

Figure 4. Diffraction patterns of the trilayer precursor and PdCuAg alloy M7 after different annealing treatments.

crystalline phases. Relatively broad diffraction peaks can be seen in the as-prepared sample pattern which corresponded to metal crystallite sizes between 30 (Pd) and 50 nm (Ag) according to Scherrer's equation.[35] Two sets of broad XRD reflections evolved after 24 h annealing, which were located at lower (A set) and higher angles (B set) than the initial Pd peaks. These peaks were even broader than those of the pure metal deposits likely due to gradually changing compositions in the early alloying stages. The double peaks show that separate Ag-rich (A set) and Cu-rich phases (B set) formed initially during alloying of the trilayers. Obviously PdAg and AgCu alloys will form first at the Pd−Ag and Ag−Cu interfaces because of the metal plating sequence. However, neither Cu nor Ag can dissociate H_2, while the membranes exhibited appreciable H_2 permeation rates even after very short alloying times (Figure 3). Thus, some Pd must have reached the membrane surface at that point already and consequently included in the B phases. Only one fcc pattern remained after 120 h, but the XRD peak widths indicated that compositional homogeneity of the PdAgCu alloy was still rather poor. For comparison, we annealed another sample at 1073 K in N_2 for 60 h in the same manner as the cutoff pieces of other membranes. This treatment gives a single fcc diffraction pattern with narrow peaks, indicating a rather homogeneous alloy with an average crystallite size of ca. 80 nm.

The double phase evolution in the early alloying stages is a reflection of the nearly complete immiscibility of Ag and Cu in the solid state. The phase diagram in Figure 5 shows that this

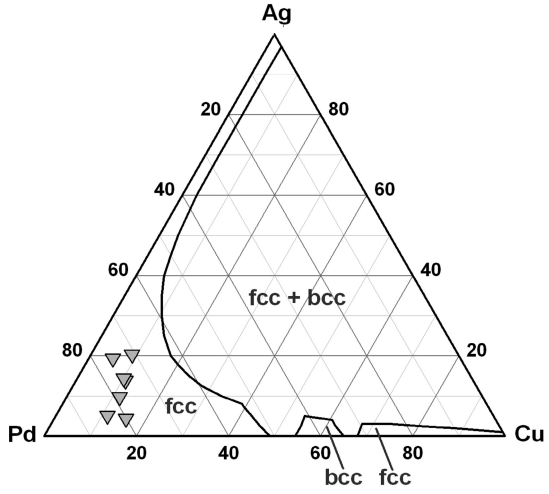

Figure 5. Isothermal section of the Pd−Ag−Cu phase diagram at 773 K after Kubashewski et al.[37] The here studied PdCuAg alloy membranes (triangles) are located in the homogeneous Pd-rich corner of this system.

miscibility gap continues deep into the Pd−Ag−Cu system at 773 K,[36,37] i.e., up to Pd contents of ca. 63%. The stoichiometry of all here investigated ternary membranes falls into the Pd-rich corner with continuous solid solutions. However, formation of these alloys has to proceed along the two-phase region boundaries at our annealing temperatures. Thus, two types of ternary crystallites with very different composition grew in the early alloying stage. This introduces a lateral element of heterogeneity within the hydrogen-selective metal layer.

Such initial stoichiometric inhomogeneity has been previously observed during preparation of PdCu membranes from separate metal layers due to a miscibility gap between intermediately formed bcc and fcc phases (cf. Pd−Cu axis in

Figure 5).[38] Note also that transient bcc phases have been observed when altogether 25 μm thick Pd/Ag/Cu trilayers with small Ag but large Cu contents were alloyed at 773 K.[18] The compositional divergence will be more severe during formation of PdCuAg than PdCu alloys because the Ag−Cu miscibility gap is much wider than the bcc−fcc ones (Figure 5). Presumably, this initial stoichiometric inhomogeneity contributed to the overly long stabilization time of H_2 permeation rates during alloy formation at 773 K. The sudden jumps of J_{H2} and E_{act} probably signal the eventual dispersal of less permeable Cu-rich phases (vide infra). Formation of transient phases with excessively diverging stoichiometry can be largely avoided if a sufficiently thick Pd layer is plated between Ag and Cu. In that case PdAg and PdCu alloys will be formed initially along the binary axes of the phase diagram in Figure 5. These can coalesce at 773 K without causing transient lateral inhomogeneity if Pd exceeds 60% in both intermediate binary layers.

3.3. Permeation Characteristics. The alloy layers were deemed to be practically homogeneous after J_{H2} and E_{act} had become stable during annealing at 773−823 K. Thereafter H_2 permeation rates were measured between 473 and 823 K and corrected for leak flow contributions using N_2 permeation data and mass transport resistance of the support following Burggraaf and co-workers[39] (cf. Supporting Information for detailed description including Figures S1−S3 and Tables S1 and S2). Figure 6 shows Arrhenius plots of the corrected H_2 fluxes obtained at ΔP_{H2} = 100 kPa, which were normalized to membrane thickness d according to

$$J_d = J_{H2}d = J_{d0}\exp[-E_{act}/RT] \quad (4)$$

The fluxes of all membranes exhibited linear temperature dependencies in this presentation. Linear regression analysis yielded the kinetic parameters of the corresponding permeation laws, i.e., E_{act} and pre-exponential factor J_{d0}, which are summarized in Table 2. This table includes also permeation

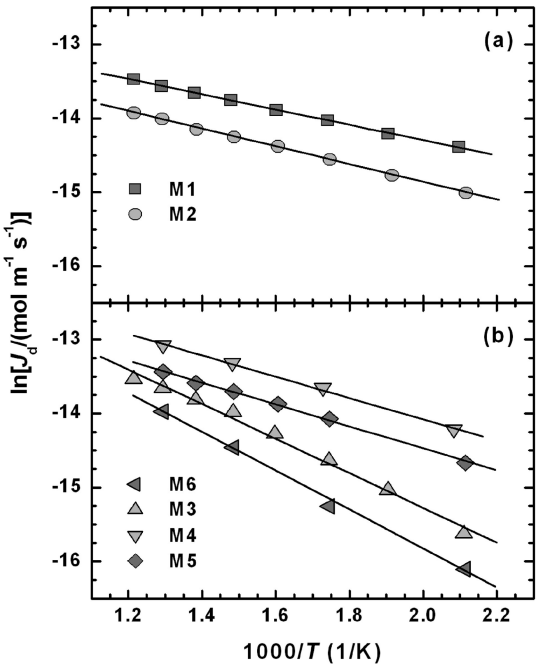

Figure 6. Temperature dependence of H_2 permeation rates of membranes (a) M1 and M2 and (b) M3−M6 after fluxes had become stable during annealing at 773 and 823 K.

kinetic data of PdCuAg membranes available in the literature. Ideal H_2/N_2 selectivity of the here investigated membranes ranged between 47 and 678 at 673 K and ΔP = 100 kPa after alloying was completed. Hydrogen permeation rates grew with pressure exponent n between 0.61 and 0.65. Such small deviations from square root pressure dependence for hydrogen diffusion-limited permeation rates have been often observed[40] including 1 mm thick Pd membranes[41] and can be attributed to nonideality of the hydrogen solutions at employed H_2 pressures.[41] Notwithstanding, we calculated permeability values P_e for n = 0.5 at 673 K and ΔP_{H2} = 100 kPa which are included in Table 2 for ease of comparison with the literature.

Table 2 and Figure S4 (Supporting Information) show that H_2 permeability improves in general with increasing Ag and decreasing Cu content of membranes as predicted by DFT calculations.[16] Membranes M2 and M4 with nearly even Ag and Cu amounts appear to be outliers since those calculations do not indicate a deviation from this general trend for such alloys. The relatively low permeability of M2 could be rooted in a flawed thickness value of the ternary alloy layer. There the thickness of the detached alloy layer amounted to ca. 50% of the initial estimate based on the weight gain of the support after metal deposition. For the other membranes the thickness of the detached layer ranged between 78% and 85% of this initial estimate. This suggests that the M2 alloy layer was uncharacteristically thin for unknown reasons at the membrane end from which the tabulated PdCuAg thickness was determined. Thus, M2 alloy thickness could have been 50−60% larger in the central membrane section which was used for permeation experiments. The cause is less clear for the apparently rather high M4 permeability. Of course, M4 PdCuAg layer thickness could be overestimated, but this membrane was also by far the shortest one due to several additional Pd and Ag plating steps with subsequent intermediary analyses of cutoff pieces. M4 further exhibited the largest discrepancy between EDS and XRD analyses (Table 1). Thus, membrane M4 characterization involves the largest experimental uncertainties of this study.

The H_2 permeabilities of PdCuAg membranes fall between those of supported PdCu and PdAg membranes prepared analogously in our laboratory. For example, a 5.5 μm thick supported $Pd_{70}Cu_{30}$ membrane had a permeability of 3.5 × 10^{-9} mol m^{-1} s^{-1} $Pa^{-0.5}$ at 673 K, and one with a ca. 3 μm thick $Pd_{75}Ag_{25}$ layer yielded 1.6 × 10^{-8} mol m^{-1} s^{-1} $Pa^{-0.5}$, while similarly thick Pd membranes exhibited values around 1.0 × 10^{-8} mol m^{-1} s^{-1} $Pa^{-0.5}$.[26,42] Evidently, addition of a small Ag portion enhances the permeability of Cu-rich alloys only marginally with regard to that of $Pd_{70}Cu_{30}$ ones, which are the current standard for sulfur-tolerant Pd alloy membranes. This is consistent with aforementioned DFT calculations.[16] On the other hand, replacement of a little Ag with Cu leads to ca. 50% permeability reduction in the optimum composition range of PdAg membranes around $Pd_{75}Ag_{25}$. While H_2 permeability of PdCuAg membranes with less than 10% Cu is still twice as high as that of $Pd_{70}Cu_{30}$ membranes and even approaches that of pure Pd ones, such small Cu contents do not prevent sulfide formation and deterioration of membrane performance in H_2S-contaminated hydrogen streams effectively.[20]

Table 2 and Figures S5 and S6 (Supporting Information) further show that both E_{act} and J_{d0} increase in tendency with decreasing Ag and increasing Cu content of the ternary alloy. Recently, correlation of those permeation kinetic parameters has been reported for PdAg membranes.[42] Compensation

Table 2. Characteristics of PdCuAg Membranes

membrane	composition[a] Ag %	Cu %	alloying time, day	d, μm	A, cm^2	$P_e \times 10^8$, [b] mol m^{-1} s^{-1} Pa$^{-0.5}$	$J_{d0} \times 10^5$, mol m^{-1} s^{-1}	E_{act}, kJ mol^{-1}	n value	H_2/N_2 selectivity[c]	origin
M1	20.4	8.9	49	4.4	18.1	0.80	0. 52	8.8	0.63	47	this work
M5	19.4	5.2	90	3.8	11.9	0.85	1.10	12.6	0.61	678	this work
M2	13.9	10.7	64	2.5	18.1	0.50	0.42	10.2	0.63	221	this work
M4	9.8	11.5	42	4.6	6.2	1.23	1.53	12.5	0.63	269	this work
M3	5.1	11.2	48	3.5	34.2	0.62	2.74	19.8	0.65	663	this work
M6	4.3	15.6	36	3.3	26.4	0.40	2.73	22.0		238	this work
P1	10.9	3.6		2.2		0.78	0.76[d]	11.3[d]		~10 000	ref 20
P2	6	20		2.1		0.44	36.3[e]	36.1		>10 000	ref 19
P3	1	20		1.9		0.50	9.05[e]	27.6		>10 000	ref 19
T1	7	25		25		0.36[d]	10.3[f]	30.0		>10000[g]	ref 17
T2	not detailed			27		0.28[d]	2.89[f]	24.5		~300[g]	ref 17

[a]Average of top and bottom end XRD analyses for membranes M1−M6. [b]At 673 K. [c]At 673 K and ΔP = 100 kPa. [d]Derived from Table 2 of ref 20. [e]Derived from P_e and E_{act} at ΔP = 100 kPa. [f]Estimated from Figure 8 of ref 17. [g]At 723 K.

between pre-exponential factor and activation energy is often observed for related thermally activated processes as a reflection of compensation between enthalpy and entropy of activation.[43] In catalysis it is known as the isokinetic relationship and in condensed matter physics as the Meyer−Neldel rule.[43] The logarithmic pre-exponential factor ln A_j varies linearly with activation energy E_j according to

$$\ln A_j = \alpha + \beta E_j \quad (5)$$

if such compensation occurs within a family of processes[43,44] where the index j denotes the individual processes. Equation 5 implies that Arrhenius plots of the related processes intersect at a single point which is defined by the intercept $\alpha = \ln k_c$ and slope $\beta = 1/RT_c$. If that is exactly fulfilled the characteristic temperature T_c will be called isokinetic temperature because all processes exhibit the same kinetic rate k_c at that temperature.[43,44]

Figure 7 shows a plot of ln J_{d0} vs E_{act} from the PdCuAg membranes listed in Table 2. Obviously these permeation kinetic parameters exhibit compensation too. Linear fitting yields $\alpha = -13.45 \pm 0.25$ and $\beta = (1.45 \pm 0.14) \times 10^{-4}$ mol J^{-1} corresponding with T_c = 828 K and k_c = 1. 44 × 10^{-6} mol m^{-1} s^{-1}. However, it is not clear whether eq 5 is exactly obeyed because of the data scatter. The scatter of kinetic parameters from the here prepared membranes is mainly due to aforementioned uncertainties about alloy layer thickness and composition, but varying support characteristics may have contributed there too. Those variations are difficult to avoid during preparation of alloy layers on porous substrates via sequential ELP, especially if very thin membranes are prepared as in the present study. In contrast, thickness and initial metal distribution are rather even in the free-standing alloy films studied at SINTEF because they were prepared by simultaneous sputtering of the metals onto polished single-crystal silicon wafers.[19,20] Therefore, such membranes are better suited for examining how well eq 5 is obeyed by the hydrogen permeation kinetics of PdCuAg alloys. Intriguingly, linear regression analysis of the three SINTEF membranes' kinetic parameters shows practically exact agreement with eq 5 as indicated by minimal errors of $\alpha = -13.56 \pm 0.08$ and $\beta = (1.57 \pm 0.03) \times 10^{-4}$ mol J^{-1}. Hence, the hydrogen permeation kinetics of Pd-rich ternary alloys with Cu and Ag might practically fulfill the isokinetic relationship, that is, such ternary membranes exhibit the same permeation rate at T_c = 773 K if normalized to thickness, i.e., k_c = 1.3 × 10^{-6} mol m^{-1} s^{-1}.

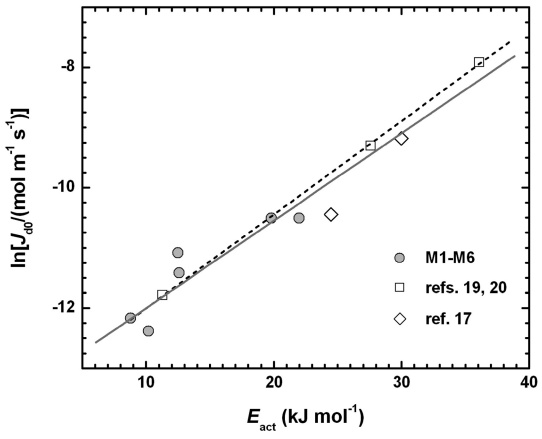

Figure 7. Correlation of the activation energy and pre-exponential factor for H_2 permeation of PdCuAg membranes. The solid line is a linear fit of the whole data set. The dashed line is a linear fit of the parameters derived for free-standing PdCuAg films from refs19 and 20.

Note that T_c is close to the temperatures at which we alloyed the Pd/Cu/Ag precursor layers. The parallel increase of J_{H2} and E_{act} (temporary) during alloy formation (Figure 3) could be due to that fact. Figure S7 (Supporting Information) demonstrates that in a PdCuAg mixed phase system Ag-rich phases with low E_{act} will exhibit higher permeability below the isokinetic temperature while Cu-rich phases with higher E_{act} will have higher permeability above that temperature. Around the isokinetic temperature actual H_2 permeation rates and energetics will depend on the shifting balance between initial Ag and Cu-rich phases and PdCuAg alloys that fall in the here investigated range. When the latter become dominant E_{act} will probably temporarily increase because the Cu content of those not yet fully homogenized PdCuAg alloys is higher than that of the initial Ag-rich alloys (cf. Figures S5 and S6, Supporting Information), while J_{H2} will grow because the fraction of less permeable Cu-rich alloys decreases in parallel.

Using hydrogen diffusion in amorphous silicon as an example Jackson showed that multiple-trapping-dominated transport quantities exhibit a Meyer−Neldel relation.[45] The characteristic parameters are related to the energy distribution of trapping sites and microscopic transport properties then.[45] Hydrogen

permeation through Pd-type membranes falls into this category as transport proceeds between interstitial binding sites for hydrogen in metal lattices.[16] Atomic diffusion in the bulk metal is the permeation rate-determining step except for very thin or contaminated membranes where surface processes can be important.[46] Surface processes typically impact H_2 permeation rates at lower temperatures, leading to a marked change in the temperature dependence[46] and a substantial increase of the low-temperature activation energy, in agreement with our experience.[38,47,48] This is obviously not the case for the here studied PdCuAg membranes (Figure 6). Thus, the permeation kinetic compensation evident in Figure 7 should originate from the energetics of hydrogen transport in the bulk alloy.

Permeation rates in metal layers are determined by the product of hydrogen solubility and diffusivity.[2,42] Therefore, two thermally activated processes factor into the observed kinetic compensation. Unfortunately, neither H diffusion energetics nor H dissolution energetics are known for PdCuAg alloys. They have been studied for PdAg alloys as a function of alloy stoichiometry, on the other hand, and it was shown that characteristic temperatures are rather similar for compensation in the hydrogen permeation kinetics (T_c = 1223 K), dissolution thermodynamics (T_c = 1150−1238 K), and diffusion kinetics (T_c = 1496 K).[42] Hence, both H dissolution and diffusion can be expected to contribute to the hydrogen permeation kinetic compensation in PdCuAg membranes too.

Hydrogen solubility is determined by the binding energies in interstitial metal lattice sites, while hydrogen diffusivity is governed by activation energies i.e., the difference between binding energies and transition state energies.[16] DFT calculations indicate that H binding energies in PdCuAg alloys decrease approximately linearly with increasing lattice constant (i.e., alloy composition) for different types of interstitial lattice sites.[16] However, they become less favorable with increasing number of Ag atoms in the nearest neighbor shell of interstitial sites, while the effect of Cu neighbors is less significant.[16] The transition state energies vary in an analogous albeit weaker manner with lattice constant.[16] Again, activation barriers for H diffusion are much larger in the immediate vicinity of Ag atoms, while Cu neighbors have a negligible effect.[16] Consequently, activation barriers for H diffusion in PdCuAg alloys tend to increase moderately with increasing Ag and decreasing Cu content,[16] while enthalpies for H dissolution will exhibit a stronger trend in the opposite direction. Since activation energies for hydrogen permeation result from the sum of those two energy terms[2,42] it is clear that they should display a similar tendency as the hydrogen binding energies as a function of lattice constant (or alloy composition).

Figure 8 shows that this is indeed the case as the E_{act} values decrease with increasing lattice constants. Accordingly, the H_2 permeation energetics and thus permeation itself are dominated by H solution thermodynamics in the investigated PdCuAg membrane range in agreement with conclusions of the DFT study.[16] It needs to be emphasized that Figure 8 depicts only an overall trend. It does not imply that the activation energy for H_2 permeation is strictly determined by the alloy lattice constant. For example, from eq 2 follows that alloys with a Ag/Cu ratio ≈ 1.4 (e.g., $Pd_{88}Cu_5Ag_7$, $Pd_{76}Cu_{10}Ag_{14}$, $Pd_{64}Cu_{15}Ag_{21}$) have isometric metal lattices with practically the same lattice constant as Pd. Obviously, the distribution among types of interstitial binding sites and transition states must differ between these alloys. The net enthalpy for H dissolution will vary accordingly and the net activation energy for H diffusion as well. It is likely that those changes are also reflected in the balance of those energies to some degree. The variations in the permeation kinetics of such membranes certainly merit further investigation.

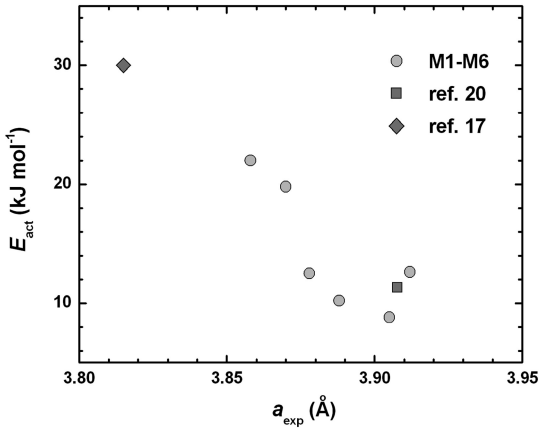

Figure 8. Correlation between the activation energy for hydrogen permeation and the experimental lattice constant of PdCuAg membranes.

Quantitative structural and permeation kinetic correlations in multicomponent alloy membranes have both practically and scientifically enormous value. From a mechanistic perspective permeation kinetic compensation implies that hydrogen transport is governed by the same rate-determining, thermally activated process step in the series of membranes under consideration. Here it means that H diffusion in the bulk remains the predominant transport step in Pd-rich PdCuAg membranes down to a layer thickness of 2 μm. Conversely, the compensation effect provides a basis for consistency checks of performance data from membranes with differing makeup. Interestingly, the permeation kinetic parameters of free-standing PdCuAg membranes[19,20] and ones supported on porous stainless steel[17] and ceramic substrates are rather consistent (Figure 7). This corroborates that support transport resistance has a minor influence on overall hydrogen permeation rates under the investigated conditions, which were similar in all three studies.

Yet, the greatest benefit of systematic relationships lies in their predictive power. Correlations between the hydrogen permeability and associated activation energy on one hand and the lattice parameter on the other have been recently explored for Pd alloys in general,[19] demonstrating the great interest in such interdependencies. In this respect the structure−function relationship depicted in Figure 8 is very intriguing because the lattice constant of an unknown PdCuAg alloy can be accurately derived according to Vegard's law (eq 2). Thus, E_{act} can be estimated a priori within a reasonably narrow range for such a membrane and by extension via eq 5 its permeability at a given temperature. Both lattice constants and activation energies for hydrogen permeation can be measured independently and with high accuracy. Therefore, such structure−function relationships can be established with good reliability through investigation of a few well-chosen alloy compositions if they existed for other multicomponent Pd alloy membranes.

4. CONCLUSIONS

A structure−function relationship has been derived for hydrogen-selective PdCuAg membranes with at least 70% Pd

on the basis of systematic correlations determined from structural and permeation kinetic analyses.

First, it has been demonstrated that the structure of PdCuAg alloys can be well described by Vegard's law. The slight lattice expansion in the here prepared membranes can be ascribed to insufficient curing of growth-related lattice defects and distortions at the employed alloy formation temperatures.

Second, detailed analysis of the hydrogen permeation kinetics has revealed compensation between activation energy and corresponding pre-exponential factor of the H_2 permeation laws obtained for membranes with differing alloy stoichiometry. This analysis encompassed literature data of PdCuAg membranes[17,19,20] demonstrating the consistency of the available permeation data of alloys within the whole composition range. The compensation effect indicates that atomic H diffusion in the bulk PdCuAg alloys remains the permeation rate-determining step down to 2 μm membrane thickness.

Third, the activation energy for H_2 permeation declines with increasing PdCuAg lattice constant, in general. This is in agreement with trends for H binding energies in interstitial lattice sites and transition states of PdCuAg alloys observed in DFT calculations.[16] In combination the three correlations enable an a priori assessment of the hydrogen permeation characteristics of PdCuAg alloys and thus facilitate rational design of such membranes.

However, alloy formation from separately deposited Pd, Ag, and Cu layers proved to be time consuming due to a wide miscibility gap in the PdCuAg phase diagram at practically feasible operation temperatures of thin-layered Pd alloy/alumina composite structures (<823 K). This gap results from the almost complete immiscibility of Cu and Ag at low temperatures. The gap and associated inhomogeneity may be largely circumvented by plating Pd layers between Ag and Cu layers, thus forming fully miscible Pd-rich PdAg and PdCu alloys initially.

■ ASSOCIATED CONTENT

Supporting Information

Additional information, figures and tables concerning correction of H_2 permeation data and structure−function relationships. This material is available free of charge via the Internet at http://pubs.acs.org.

■ AUTHOR INFORMATION

Corresponding Author

*E-mail: goldbach@dicp.ac.cn.

Notes

The authors declare no competing financial interest.

■ ACKNOWLEDGMENTS

Financial support by the European Union through FP7 project CACHET II (contract no. 241342, http://www.cachet2.eu) and the Chinese Academy of Sciences through the External Cooperation Program (Helmholtz-CAS Joint Research Group on Integrated Catalytic Technologies for Efficient Hydrogen Production, grant no. GJHZ1304) is gratefully acknowledged. We are also indebted to ECN and Dr. F. van Berkel for providing ceramic support membranes and seals.

■ REFERENCES

(1) Yun, S.; Oyama, S. T. Correlations in Palladium Membranes for Hydrogen Separation: A Review. *J. Membr. Sci.* **2011**, *375*, 28−45.
(2) Shu, J.; Grandjean, B.; van Neste, A.; Kaliaguine, S. Catalytic Palladium-Based Membrane Reactors: A Review. *Can. J. Chem. Eng.* **1991**, *69*, 1036−1060.
(3) Gallucci, F.; Fernandez, E.; Corengia, P.; van Sint Annaland, M. Recent Advances on Membranes and Membrane Reactors for Hydrogen Production. *Chem. Eng. Sci.* **2013**, *92*, 40−66.
(4) Lin, Y.-M.; Liu, S.-L.; Chuang, C.-H.; Chu, Y.-T. Effect of Incipient Removal of Hydrogen through Palladium Membrane on the Conversion of Methane Steam Reforming: Experimental and Modeling. *Catal. Today* **2003**, *82*, 127−139.
(5) Liu, P. K. T.; Sahimi, M.; Tsotsis, T. T. Process Intensification in Hydrogen Production from Coal and Biomass Via the Use of Membrane-Based Reactive Separations. *Curr. Opin. Chem. Eng.* **2012**, *1*, 342−351.
(6) Mundschau, M.; Xie, X.; Evenson, C.; Sammells, A. Dense Inorganic Membranes for Production of Hydrogen from Methane and Coal with Carbon Dioxide Sequestration. *Catal. Today* **2006**, *118*, 12−23.
(7) Kajiwara, M.; Uemiya, S.; Kojima, T. Stability and Hydrogen Permeation Behavior of Supported Platinum Membranes in Presence of Hydrogen Sulfide. *Int. J. Hydrogen Energy* **1999**, *24*, 839−844.
(8) Kulprathipanja, A.; Alptekin, G. O.; Falconer, J. L.; Way, J. D. Pd and Pd-Cu Membranes: Inhibition of H_2 Permeation by H_2S. *J. Membr. Sci.* **2005**, *254*, 49−62.
(9) McKinley, D. L. Metal Alloy for Hydrogen Separation and Purification. U.S. Patent 3350845, July, 11, 1967.
(10) Edlund, D. A Membrane Reactor for H_2S Decomposition. *Proceedings of Advanced Coal-Fired Power Systems '96 Review Meeting*, DOE/ER/81419-97/C0749, U.S. DOE, Morgantown, WV, 1996; pp 1−9.
(11) Morreale, B. D.; Ciocco, M. V.; Howard, B. H.; Killmeyer, R. P.; Cugini, A.; Enick, R. M. Effect of Hydrogen-Sulfide on the Hydrogen Permeance of Palladium-Copper Alloys at Elevated Temperatures. *J. Membr. Sci.* **2004**, *241*, 219−224.
(12) Pomerantz, N.; Ma, Y. H. Novel Method for Producing High H_2 Permeability Pd Membranes with a Thin Layer of the Sulfur Tolerant Pd/Cu Fcc Phase. *J. Membr. Sci.* **2011**, *370*, 97−108.
(13) Peters, T. A.; Kaleta, T.; Stange, M.; Bredesen, R. Hydrogen Transport through a Selection of Thin Pd-Alloy Membranes: Membrane Stability, H_2S Inhibition, and Flux Recovery in Hydrogen and Simulated WGS Mixtures. *Catal. Today* **2012**, *193*, 8−19.
(14) Wieland, S.; Melin, T.; Lamm, A. Membrane Reactors for Hydrogen Production. *Chem. Eng. Sci.* **2002**, *57*, 1571−1576.
(15) Pan, X.; Kilgus, M.; Goldbach, A. Low-Temperature H_2 and N_2 Transport through Thin $Pd_{66}Cu_{34}H_x$ Layers. *Catal. Today* **2005**, *104*, 225−230.
(16) Ling, C.; Semidey-Flecha, L.; Sholl, D. S. First-Principles Screening of PdCuAg Ternary Alloys as H_2 Purification Membranes. *J. Membr. Sci.* **2011**, *371*, 189−196.
(17) Tarditi, A. M.; Braun, F.; Cornaglia, L. M. Novel PdAgCu Ternary Alloy: Hydrogen Permeation and Surface Properties. *Appl. Surf. Sci.* **2011**, *257*, 6626−6635.
(18) Tarditi, A. M.; Cornaglia, L. M. Novel PdAgCu Ternary Alloy as Promising Materials for Hydrogen Separation Membranes: Synthesis and Characterization. *Surf. Sci.* **2011**, *605*, 62−71.
(19) Peters, T. A.; Kaleta, T.; Stange, M.; Bredesen, R. Development of Thin Binary and Ternary Pd-Based Alloy Membranes for Use in Hydrogen Production. *J. Membr. Sci.* **2011**, *383*, 124−134.
(20) Peters, T. A.; Kaleta, T.; Stange, M.; Bredesen, R. Development of Ternary Pd-Ag-TM Alloy Membranes with Improved Sulphur Tolerance. *J. Membr. Sci.* **2013**, *429*, 448−458.
(21) Nayebossadri, S.; Speight, J.; Book, D. Effects of Low Ag Additions on the Hydrogen Permeability of Pd−Cu−Ag Hydrogen Separation Membranes. *J. Membr. Sci.* **2014**, *451*, 216−225.
(22) Bonekamp, B. C.; van Horssen, A.; Correia, L. A.; Vente, J. F.; Haije, W. G. Macroporous Support Coatings for Molecular Separation

Membranes Having a Minimum Defect Density. *J. Membr. Sci.* **2006**, *278*, 349−356.
(23) Hou, S.; Jiang, K.; Li, W.; Xu, H.; Yuan, L. Preparation Method of a Metal Palladium Composite Membrane or Alloy Palladium Composite Membrane. European Patent 1701779 B1, Apr 8, 2010.
(24) Zeng, G.; Goldbach, A.; Xu, H. Impact of Support Mass Flow Resistance on Low-Temperature H_2 Permeation Characteristics of a $Pd_{95}Ag_5/Al_2O_3$ Composite Membrane. *J. Membr. Sci.* **2009**, *326*, 681−687.
(25) Zeng, G.; Goldbach, A.; Shi, L.; Xu, H. On Alloying and Low-Temperature Stability of Thin, Supported PdAg Membranes. *Int. J. Hydrogen Energy* **2012**, *37*, 6012−6019.
(26) Yuan, L.; Goldbach, A.; Xu, H. Real-Time Monitoring of Metal Deposition and Segregation Phenomena During Preparation of PdCu Membranes. *J. Membr. Sci.* **2008**, *322*, 39−45.
(27) Li, H.; Goldbach, A.; Li, W.; Xu, H. PdC Formation in Ultra-Thin Pd Membranes During Separation of H_2/CO Mixtures. *J. Membr. Sci.* **2007**, *299*, 130−137.
(28) Hydrogen (nominal purity > 99%) might contain N_2 and CO_2 as main impurities according to supplier specification. However, we did not detect any impurities in the employed H_2 via gas chromatographic analyses.
(29) Vegard, L. The Constitution of the Mixed Crystals and the Filling of Space of the Atoms. *Z. Phys.* **1921**, *5*, 17−26.
(30) Raub, E.; Wörwag, G. Die Silber-Palladium-Kupfer-Legierungen. *Z. Metallkd.* **1955**, *46*, 52−57.
(31) Tosques, J.; Martin, M. H.; Roué, L.; Guay, D. Hydrogen Solubility in PdCuAg Ternary Alloy Films Prepared by Electrodeposition. *Int. J. Hydrogen Energy* **2014**, *39*, 15810−15818.
(32) Guerreiro, B. H.; Martin, M. H.; Roue, L.; Guay, D. Hydrogen Solubility in PdCuAu Alloy Thin Films Prepared by Electrodeposition. *Int. J. Hydrogen Energy* **2014**, *39*, 3487−3497.
(33) Galipaud, J.; Martin, M. H.; Roué, L.; Guay, D. Measurement of Hydrogen Solubility in Pd_xCu_{100-X} Thin Films Prepared by Pulsed Laser Deposition: An Electrochemical in Situ X-Ray Diffraction Analysis. *J. Phys. Chem. C* **2013**, *117*, 2688−2698.
(34) Hollemann, A. F.; Wiberg, N. *Lehrbuch der Anorganischen Chemie*; Walter de Gruyter, Berlin, 1985; p 720.
(35) Cullity, B. D. *Elements of X-ray Diffraction*; Addison-Wesley: New York, 1978; pp 101−102.
(36) Raub, E. Alloys of the Platinum Group Metals. Summary of the Last Years Work. *Rev. Metall.* **1955**, *52*, 429−440.
(37) Kubashewski, O.; Semenova, E.; Ilyenko, S. Silver−Copper−Palladium. In *Noble Metal Ternary Systems: Phase Diagrams, Crystallographic and Thermodynamic Data*; Effenberg, G., Ilyenko, S., Eds.; SpringerMaterials-The Landolt-Börnstein Database; Springer: Berlin, Heidelberg, 2006; p 135−143. (http://www.springermaterials.com). DOI: 10.1007/10916070_14.
(38) Yuan, L.; Goldbach, A.; Xu, H. Segregation and H_2 Transport Rate Control in Body-Centered Cubic PdCu Membranes. *J. Phys. Chem. B* **2007**, *111*, 10952−10958.
(39) Keizer, K.; Uhlhorn, R. J. R.; Van vuren, R. J.; Burggraaf, A. J. Gas Separation Mechanisms in Microporous Modified Gamma Alumina Membranes. *J. Membr. Sci.* **1988**, *39*, 285−300.
(40) Rothenberger, K.; Cugini, A.; Howard, B.; Killmeyer, R.; Ciocco, M.; Morreale, B.; Enick, R.; Bustamante, F.; Mardilovich, I.; Ma, Y. High Pressure Hydrogen Permeance of Porous Stainless Steel Coated with a Thin Palladium Film Via Electroless Plating. *J. Membr. Sci.* **2004**, *244*, 55−68.
(41) Morreale, B. D.; Ciocco, M. V.; Enick, R. M.; Morsi, B. I.; Howard, B. H.; Cugini, A. V.; Rothenberger, K. S. The Permeability of Hydrogen in Bulk Palladium at Elevated Temperatures and Pressures. *J. Membr. Sci.* **2003**, *212*, 87−97.
(42) Zeng, G.; Goldbach, A.; Shi, L.; Xu, H. Compensation Effect in H_2 Permeation Kinetics of PdAg Membranes. *J. Phys. Chem. C* **2012**, *116*, 18101−18107.
(43) Yelon, A.; Sacher, E.; Linert, W. Comment on "The Mathematical Origins of the Kinetic Compensation Effect" Parts 1 and 2 by P. J. Barrie, Phys. Chem. Chem. Phys., 2012, 14, 318 and 327. *Phys. Chem. Chem. Phys.* **2012**, *14*, 8232−8234.
(44) Barrie, P. J. The Mathematical Origins of the Kinetic Compensation Effect: 1. the Effect of Random Experimental Errors. *Phys. Chem. Chem. Phys.* **2012**, *14*, 318−326.
(45) Jackson, W. Connection between the Meyer-Neldel Relation and Multiple-Trapping Transport. *Phys. Rev. B* **1988**, *38*, 3595−3598.
(46) Ward, T. L.; Dao, T. Model of Hydrogen Permeation Behavior in Palladium Membranes. *J. Membr. Sci.* **1999**, *153*, 211−231.
(47) Shi, L.; Goldbach, A.; Zeng, G.; Xu, H. H_2O_2 Synthesis over PdAu Membranes. *Catal. Today* **2010**, *156*, 118−123.
(48) Shi, L.; Goldbach, A.; Zeng, G.; Xu, H. Preparation and Performance of Thin-Layered PdAu/Ceramic Composite Membranes. *Int. J. Hydrogen Energy* **2010**, *35*, 4201−4208.